

DYNAMIC EFFECTS ON FATIGUE CRACK GROWTH

Cássio D. de Almeida, Rafael L. Moresco and Eduardo Bittencourt

*Centro de Mecânica Aplicada e Computacional, Universidade Federal do Rio Grande do Sul, Av.
Osvaldo Aranha, 99, 3º andar, Porto Alegre, RS, Brasil, cassio.dani@ufrgs.br,
rafael_moresco01@yahoo.com.br, eduardo.bittencourt@ufrgs.br,
<https://www.ufrgs.br/engcivil/ppgec/>*

Keywords Fatigue, dynamic effects, cohesive zone model.

Abstract. The influence of dynamic (inertial) effects on fatigue crack growth is studied in this paper. The crack growth zone is modeled by cohesive interfaces whose separation process is described by a fatigue cohesive zone model. Two different loading types are considered: one in which the loading increases to a maximum value in a certain time interval and the other one where loading is cyclic. Quasi-static and dynamic solutions are compared to establish the conditions in which the dynamic effects become important in the analysis. It is discussed how loading speed and frequency can modify crack growth characteristics such as, growth rate, crack extension and time for the beginning of the growth process. It is observed that high loading speeds may even change the failure mode of cracked structures from crack propagation to uniform debonding. Similarly, high loading frequencies may lead to the formation of micro cracks ahead of the crack tip. Stress distribution and crack evolution through time are also investigated.

1 INTRODUCTION

The need to evaluate the safety of cracked structures motivated the development of the fatigue and fracture mechanics fields. Crack growth may occur due to static or dynamic loading, either in one or multiple load cycles. Although the static failure mechanisms of cracked structures are well established, dynamic fatigue fracture is not yet fully understood.

Material inertia can influence crack growth when the loading is applied sufficiently fast, when the crack growth is rapid or when the material properties are strain rate dependent. If loading rate is sufficiently slow the crack tip fields will be those of static analyses and crack growth will not be affected by inertia. However if loading rate is fast, the crack tip fields and crack growth change. Additionally, material inertia will act alongside material stiffness to describe the body's motion. On the other hand rapid dynamic loading and rapid crack growth also generate stress waves because of inertial effects. This stress waves affect the near crack tip stress field and consequently, the crack growth. The influence of dynamic effects on crack propagation also depends on material properties, loading conditions and the geometry of the body.

The influence of these factors was investigated by different studies in the past. Based on energy concepts it was found that the theoretical limiting speed for a mode I crack on an elastic material is the Rayleigh wave speed (Freund, 1990). Also based on energy concepts it was established that inertial effects may not be important in determining the crack tip field as long as the crack speed is less than about one third of the elastic wave speed (Freund, 1990). The cohesive zone model (CZM) also has been used in the study of dynamic crack growth. Xu and Needleman (1994) evaluated the effects of high impact speeds on crack growth rates and crack branching. Needleman (1997) implemented the CZM to assess dynamic impact loading on elastic and viscoplastic materials. Siegmund and Needleman (1997) used the CZM to assess the effect of strain rate hardening on the near tip fields and on crack growth and arrest under dynamic impact loading. Zhou et al. (2005) successfully modeled high speed crack growth in Polymethyl Methacrylate using a rate dependent CZM. Wang and Siegmund (2006) studied size effects on fatigue crack growth for quasi-static applications by using the CZM.

Thus the present work aims to assess dynamic effects on crack propagation on an interface. A finite element analysis was conducted with the crack growth zone modeled by cohesive interfaces. Both impact and fatigue loading are studied.

2 MODEL DESCRIPTION

2.1 Cohesive zone formulation

The irreversible CZM used in this paper has been developed by Roe and Siegmund (2003) based on the cohesive model presented by Needleman (1992) and is briefly summarized in this section.

The cohesive law relates the normal and shear components of material separation, Δu_n and Δu_t , with normal and shear cohesive tractions T_n and T_t . The cohesive tractions are implemented within the finite element method (FEM) model through the principle of virtual work. The implemented model is capable of analyzing both normal and shear cohesive tractions but only normal cohesive tractions will be described here since this paper is focused on mode I loading. Therefore the traction-separation law is given by Eq. (1).

$$T_n = \sigma_{\max,0} \exp(1) \exp\left(-\frac{\Delta u_n}{\delta_0}\right) \left\{ \frac{\Delta u_n}{\delta_0} \exp\left(-\frac{\Delta u_t^2}{\delta_0^2}\right) + (1.0 - q) \frac{\Delta u_n}{\delta_0} \left[1.0 - \exp\left(-\frac{\Delta u_t^2}{\delta_0^2}\right) \right] \right\}. \quad (1)$$

The material parameters in Eq. (1) are the initial cohesive strength, $\sigma_{\max,0}$, and the cohesive length, δ_0 . The parameter q is the ratio between the normal and shear cohesive surface energies $\phi_{n,0}$ and $\phi_{t,0}$ given by Eq. (2). For mode I material separation, $\Delta u_t = 0$ and the second term inside the braces in Eq. (1) disappear. In the absence of fatigue, cohesive elements will fail when the cohesive energy is entirely consumed which is assumed to occur for $\Delta u_n = 5\delta_0$.

$$\begin{aligned} \phi_{n,0} &= \sigma_{\max,0} \delta_0 \exp(1), \\ \phi_{t,0} &= \sqrt{\frac{\exp(1)}{2}} \tau_{\max,0} \delta_0. \end{aligned} \quad (2)$$

In order to simulate fatigue effects, a cyclic damage variable D_c is introduced. This variable describes the reduction in cohesive strength due to fatigue. The current cohesive strength is then given by Eq. (3).

$$\sigma_{\max} = (1 - D_c) \sigma_{\max,0}. \quad (3)$$

The evolution of the damage variable is described by Eq. (4) where damage accumulation only occurs if $T_n / \sigma_{\max} > \sigma_f / \sigma_{\max,0}$.

$$\dot{D}_c = \frac{|\Delta \dot{\bar{u}}|}{\delta_\Sigma} \left[\frac{T_n}{\sigma_{\max}} - \frac{\sigma_f}{\sigma_{\max,0}} \right] H\left(\int_t |\Delta \dot{\bar{u}}| dt - \delta_0\right). \quad (4)$$

Where H is the Heaviside function. The variable $\Delta \dot{\bar{u}}$ is the total crack opening rate which is calculated from $\Delta \bar{u}$, the total crack opening. For mode I material separation, $\Delta \bar{u} = \Delta u_n$ and Eq. (5) defines $\Delta \dot{\bar{u}}$.

$$\Delta \dot{\bar{u}} = \Delta \bar{u}(t) - \Delta \bar{u}(t - \Delta t). \quad (5)$$

On Eq. (4) new cohesive zone parameters are introduced: δ_Σ is the accumulated cohesive length, which scales the normalized increment of the effective material separation, and σ_f is the infinite life endurance limit.

Unloading and reloading follow Eq. (6) where $T_{n,max}$ is the maximum traction corresponding to the maximum separation $\Delta u_{n,max}$ of the previous loading/unloading cycle.

$$T_n = T_{n,max} + \left(\frac{T_{n,max}}{\Delta u_{n,max}} \right) (\Delta u_n - \Delta u_{n,max}). \quad (6)$$

During unloading, contact between cohesive interfaces occur when $\Delta u_n < 0$. If the cohesive interface is not broken ($D_c < 1$) the cohesive zone behaviour under compression is given by Eq. (7) where A is taken as 30.

$$T_{n,comp} = A \cdot \sigma_{\max,0} \exp(1) \exp\left(-\frac{\Delta u_n}{\delta_0}\right) \left(\frac{\Delta u_n}{\delta_0}\right). \quad (7)$$

After the cohesive interface fails ($D_c = 1$), cohesive tensions cease to exist. In this case contact is calculated by Eq. (8) where B is taken as 10.

$$T_{n,contact} = B \cdot \sigma_{max,0} \exp(1) \exp\left(-\frac{\Delta u_n}{\delta_0}\right) \left(\frac{\Delta u_n}{\delta_0}\right). \quad (8)$$

2.2 Finite element model

Equilibrium can be represented through the principle of virtual work by Eq. (9).

$$\int_{\Omega} \sigma \left(\frac{\partial \delta U}{\partial x} \right) dV + \int_{\Omega} \rho \ddot{U} \cdot \delta U dV + \int_{\Gamma^c} T_{CZ} \cdot \delta \Delta dS = \int_{\Omega} B \cdot \delta U dV + \int_{\Gamma} F \cdot \delta U dS. \quad (9)$$

Where Ω is the body's volume, Γ is the body's external surface; Γ^C is the cohesive zone surface, σ is the Cauchy stress, U is the displacement vector, ρ is the specific mass of the material, T_{CZ} are the cohesive surface tractions, Δ is the crack opening, B are the volume forces, F are the external forces and δ is an arbitrary virtual variation. This equation can then be transformed in an ordinary differential equation by eliminating the virtual nodal displacements (Eq. (10)).

$$M\ddot{U} + F_{int} - F = 0. \quad (10)$$

Where M is the mass matrix and F_{int} are the internal forces including the cohesive tractions. The analyzed problem is depicted in Figure 1.

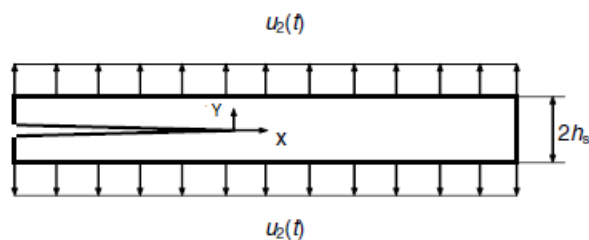


Figure 1: Model geometry.

The implemented finite element mesh is composed by 4488 4-node plane strain elements plus 141 cohesive elements inserted ahead of the crack tip. The crack is assumed to propagate along its initial direction. A highly refined mesh is placed in front of the initial crack tip with square elements of length 0.517 mm. For symmetry reasons only the top half of the specimen is modeled.

Computations were carried out for specimen's length $L=0.374$ m and height $h_s=0.075$ m. The initial crack length is one third of the specimen's length. A prescribed uniform displacement $u_2(t)$ is applied on the top and bottom edges of the specimen. The material is assumed to be homogenous isotropic elastic with Young's modulus $E=10^{11}$ Pa, Poisson's coefficient $\nu=0.34$ and specific mass $\rho=3000$ Kg/m³. Cohesive parameters are $\delta_0=10^{-4}$ m, $\sigma_{max,0}=10^9$ Pa, $\delta_{\Sigma}/\delta_0=4$, $\sigma_f/\sigma_{max,0}=0.25$. There is no concern in modeling any specific type of material.

Dynamic equations of motion were solved using an implicit time integration scheme. A consistent mass matrix was used. Time increments were chosen to accurately represent the loading frequencies and at least the first three vibration modes of the structure. Modal analysis of the specimen revealed that the fundamental frequencies for the undamaged and fully damaged (all cohesive elements failed) conditions are 2400 Hz and 1200 Hz, respectively.

3 RESULTS

3.1 Impact loading

In this first example the prescribed displacement $u_2(t)$ increases linearly from zero to a maximum value $u_{2,max}$ in a certain time interval Δt . The adopted maximum displacement value $u_{2,max} = 3.64 \times 10^{-4}$ m is the displacement for which the J-integral energy for the problem equals the normal cohesive energy. Dynamic simulations were conducted for different values of Δt and a quasi-static simulation was conducted for $\Delta t = 20$ s.

Contour plots of the vertical component of Cauchy stress σ_{22} for different total times are shown in Figures 2 and 3 for $\Delta t = 10^{-4}$ s and $\Delta t = 10^{-5}$ s respectively. For time intervals Δt equal or greater than 10^{-4} s the crack tip stress fields were found to be similar to the quasi-static case. Stress concentration near the crack tip occurs and the failure mode for these cases is crack growth. However for $\Delta t = 10^{-5}$ s the stress fields are completely different. Figure 3 clearly shows that there is a time gap in which a stress wave propagates from the loaded edges to the center of the specimen. The stress wave reaches the crack at time $t = 1.04 \times 10^{-5}$ s which is the exact time a stress wave would take to propagate through $h_s = 0.075$ m moving at the material's dilatational wave speed (Eq. (11)).

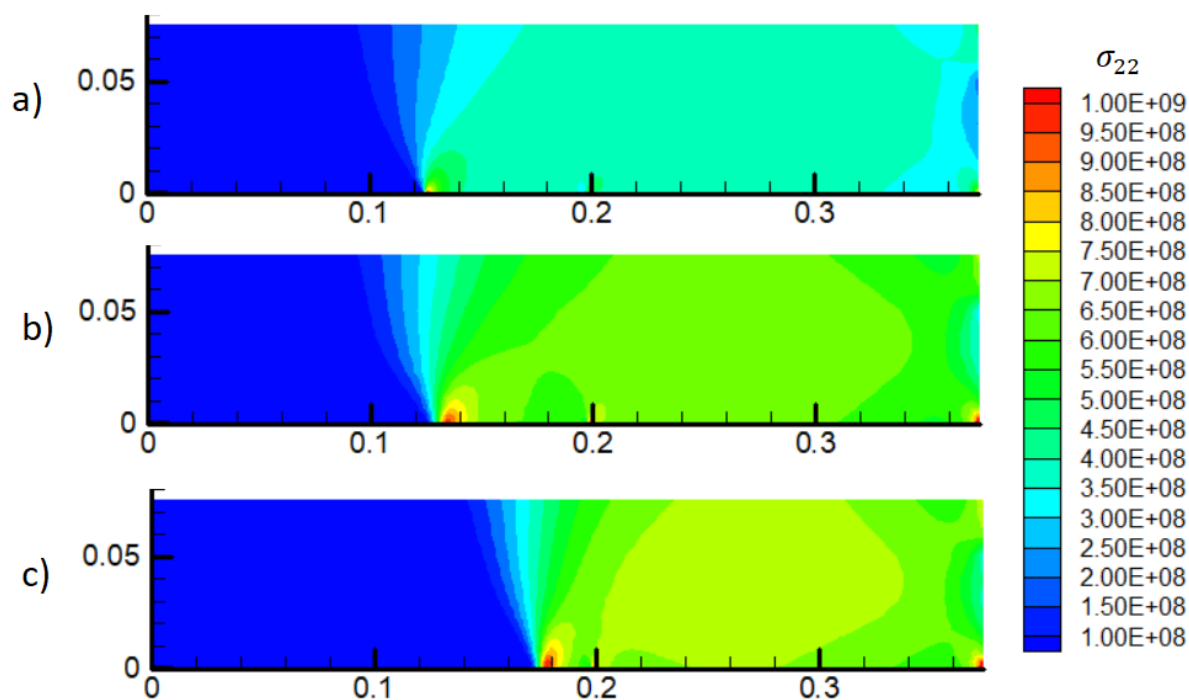


Figure 2: Vertical component of Cauchy stress σ_{22} for $\Delta t = 10^{-4}$ s. a) $t=0.54 \times 10^{-4}$ s. b) $t=0.82 \times 10^{-4}$ s. c) $t=1.1 \times 10^{-4}$ s.

$$c_d = \sqrt{\frac{E(1-\nu)}{\rho(1+\nu)(1-2\nu)}} = 7162.82 \text{ m/s} . \quad (11)$$

Figure 3 shows that decohesion occurs uniformly along the cohesive surface when the stress wave effectively reaches the crack tip. This occurs because the magnitude of the stress carried

by the wave is greater than the maximum cohesive strength of the material. In reality, the speed of crack propagation is proportional to the magnitude of the stress wave. When the magnitude of the stress wave exceeds the cohesive strength of the material, the apparent speed of propagation is infinite and the material suddenly fails. This effect was also observed by [Xu and Needleman \(1994\)](#).

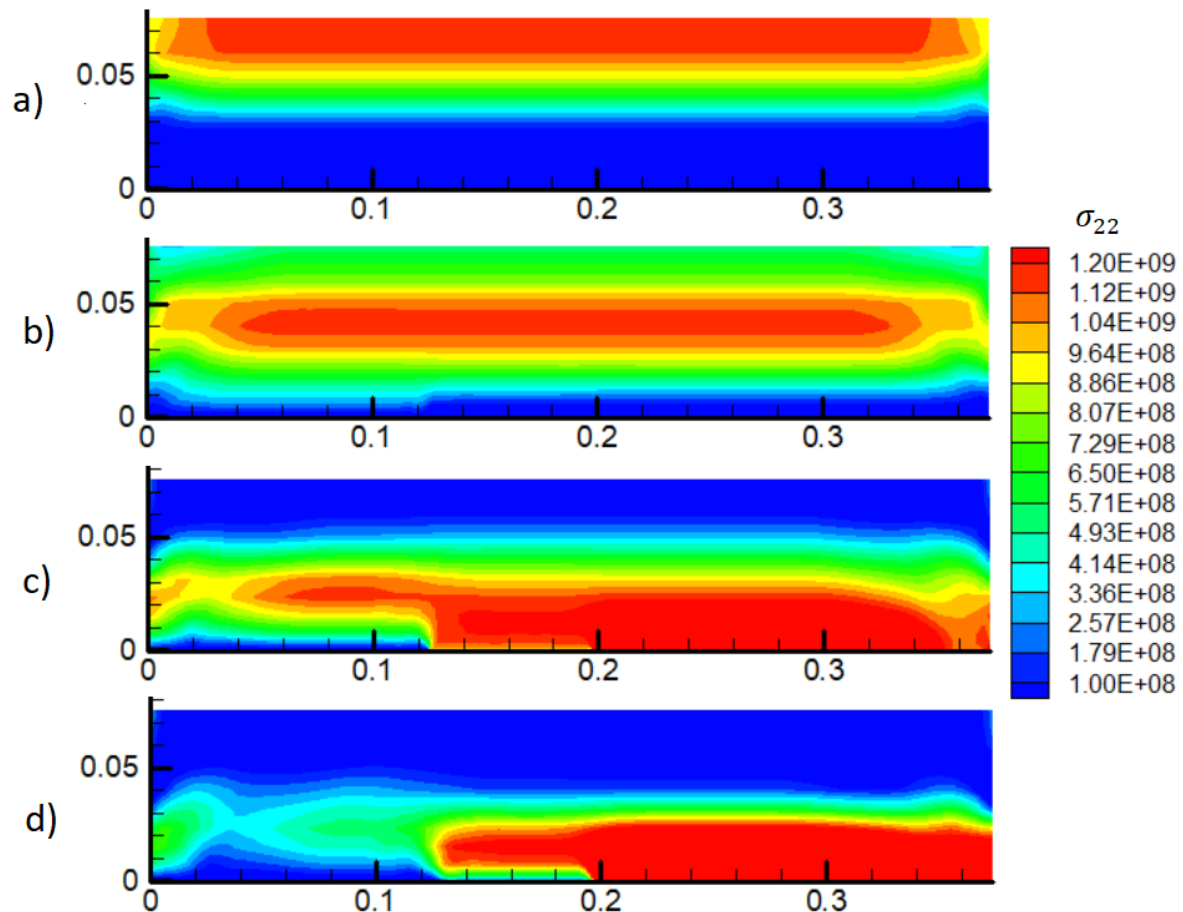


Figure 3: Vertical component of Cauchy stress σ_{22} for $\Delta t = 10^{-5}$ s. a) $t = 0.64 \times 10^{-5}$ s. b) $t = 0.96 \times 10^{-5}$ s. c) $t = 1.28 \times 10^{-5}$ s. d) $t = 1.44 \times 10^{-5}$ s.

Normalized crack extension $\Delta a/\delta_0$ as a function of the normalized time $t/\Delta t$ is shown in [Figure 4](#). Dynamic effects have a negligible influence on crack growth for time intervals Δt equal or greater than 10^{-3} s (which corresponds to an average loading speed of 0.36 m/s). For time intervals Δt less than 10^{-3} s it is immediately observed that crack extension is greater compared to the quasi-static simulation. A larger relative time gap between loading and crack growth due to inertial effects is also noticed. Additionally, a slight increase in the crack growth rate occurs with the decrease of Δt . For $\Delta t = 10^{-4}$ s and $\Delta t = 5 \times 10^{-5}$ s and after a brief acceleration phase crack tip speeds have approximately constant values of 2365 m/s and 2413 m/s respectively. These speeds are both smaller than the Rayleigh wave speed ($c_r = 3289$ m/s) and larger than one third of the uniaxial elastic wave speed ($1/3 c_l = 1925$ m/s) which is consistent with energy based predictions ([Freund, 1990](#)). The increase in the crack growth rate with the decrease of Δt occurs until Δt reaches a limiting value where the failure mode shifts from crack propagation to uniform debonding as seen in [Figure 3](#). The large time gap between

loading and the beginning of the growth process for $\Delta t = 1 \times 10^{-5}$ s is due to the time the stress wave takes to propagate through the specimen. During this time no crack growth occurs. After the stress wave finally reaches the crack there is a brief crack growth stage followed by the sudden failure of the remaining cohesive elements.

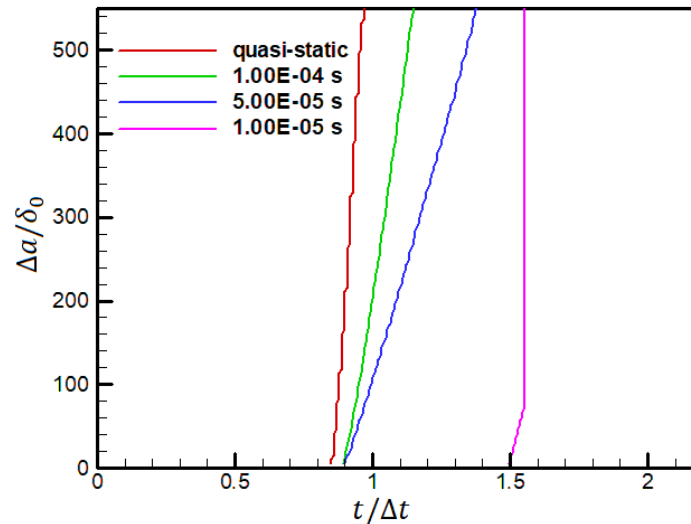


Figure 4: Normalized crack extension $\Delta a/\delta_0$ as a function of the normalized time $t/\Delta t$.

3.2 Cyclic loading

In this example the prescribed displacement $u_2(t)$ is a sinusoidal function of time that varies from zero to a maximum value $u_{2,max}$. The adopted maximum displacement value $u_{2,max} = 1.63 \times 10^{-4}$ m is the displacement for which the J-integral energy for the problem equals 20% of the normal cohesive energy. Figure 5 depicts normalized crack extension $\Delta a/\delta_0$ as a function of the number of loading cycles N . Dynamic simulations were conducted for different values of loading frequency f and a quasi-static simulation was conducted for $f = 0.05$ Hz.

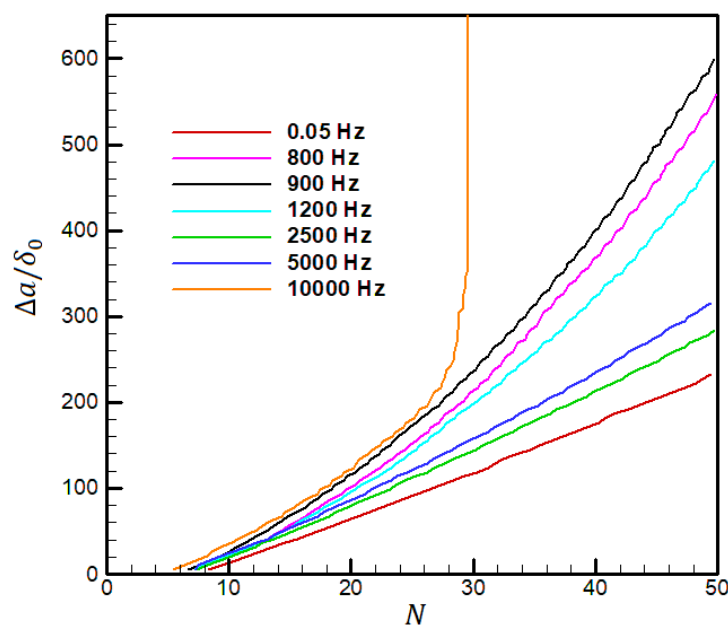


Figure 5: Normalized crack extension $\Delta a/\delta_0$ as a function of the number of cycles N .

The predicted crack growth behavior for the quasi-static simulation is very similar to that obtained by Wang and Siegmund (2006) for the same conditions. Dynamic simulations for high frequency loading showed that the incubation period that precedes crack growth is smaller compared to the quasi-static simulation. For this reason crack extension is always larger when dynamic effects are considered. Besides that, crack growth rate tends to increase with crack extension in the dynamic simulations while in quasi-static simulations it remains constant. This effect was more severe for frequencies between 800 and 1200 Hz and practically non-existent for other values of frequency. Considering that the fundamental frequency of the specimen varies from 2400 Hz to 1200 Hz, it is possible that the acceleration in crack growth is a result of a resonating frequency. For $f= 10$ kHz, a different process takes place: the crack growth rate increases abruptly and the cohesive elements fail in a smaller number of cycles. The rupture process for this frequency is explained in the following paragraphs.

Figure 6 depicts normalized crack opening $\Delta u_n/\delta_0$ as a function of normalized position x/δ_0 for different loading frequencies and number of cycles. The position x is defined by the coordinated axis in Figure 1. For $N=20.5$ cycles, all the opening profiles have the same shape. For $N=29.5$ cycles, the opening profile remains the same for the smaller frequencies, only the opening values increase. However for $f= 10$ kHz the profile is clearly different, having larger values of crack opening further away from the initial crack tip. Figure 7 depicts the damage distribution along the cohesive elements for the same number of cycles of Figure 6. Again it can be seen that for $N=20.5$ cycles the damage distribution is similar for all the frequencies. Nevertheless for $N=29.5$ cycles and $f= 10$ kHz the damage variable doesn't decrease sharply for greater values of x/δ_0 as it happens for the other frequencies. Instead the damage distribution has peak values at certain distances from the crack tip. These peak values eventually grow to a unitary value and the cohesive elements fail. This process creates a micro crack ahead of the actual crack tip and increases substantially the crack extension in a very short time interval.

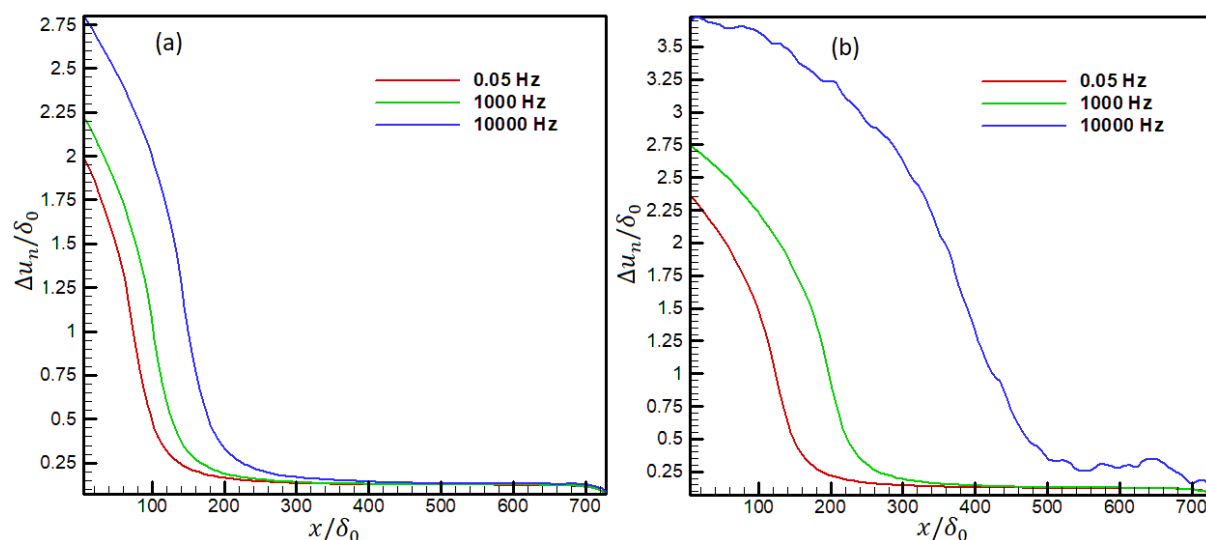


Figure 6: Crack opening profiles. a) $N=20.5$ b) $N=29.5$

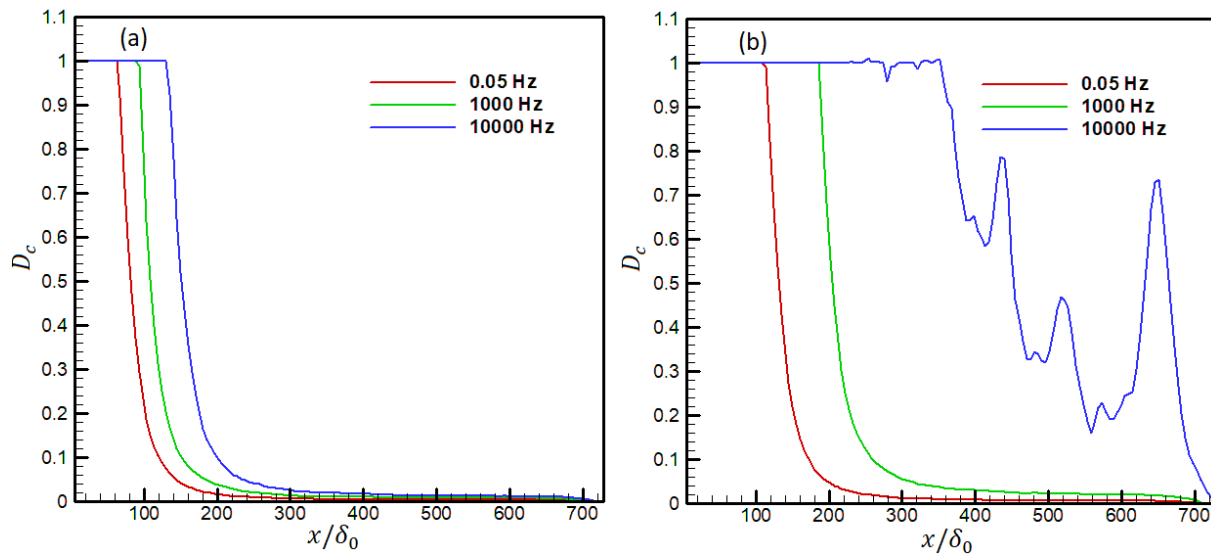


Figure 7: Damage distribution. a)N=20.5 b)N=29.5

Figure 8 is a contour plot of the vertical component of Cauchy stress σ_{22} for $f= 10$ kHz that illustrates the formation of the micro crack ahead of the actual crack tip. At $N=20.5$ cycles the stress field around the crack tip is very similar to that of Figure 2 which indicates a steady crack growth. At $N=29.5$ cycles the crack tip is located approximately 0.16m away from the left edge of the specimen but there is a stress concentration located 0.015m to the right of this position. At this stress concentration, σ_{22} surpasses the value of σ_{max} that is smaller than $\sigma_{max,0}$ due to cyclic damage. This accelerates the process of damage accumulation and quickly makes the cohesive elements fail creating a micro crack. The original crack then quickly grows through the weakened strip of cohesive elements and merges with the micro crack. Hence crack growth rate increases sharply.

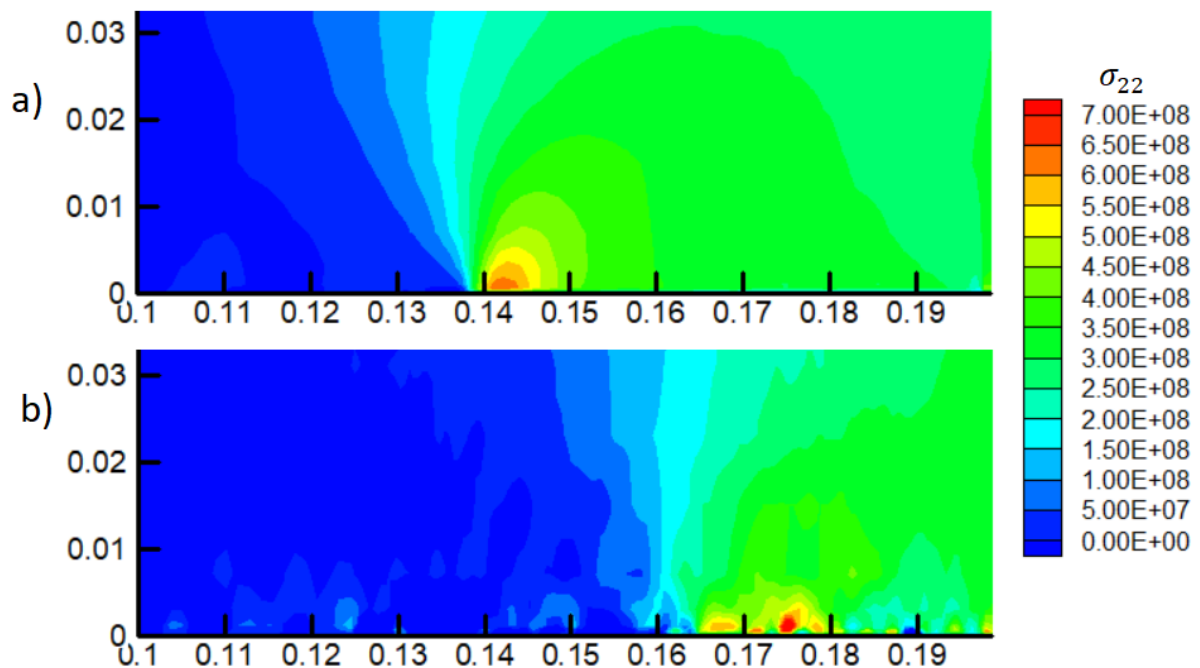


Figure 8: Vertical component of Cauchy stress σ_{22} for $f= 10$ kHz. a) N=20.5 b) N=29.5

4 CONCLUSIONS

The present computational study demonstrates that the type of failure in cracked structures may be dependent on dynamic effects. It was found that for large impact times dynamic effects were negligible. For intermediate values of impact time crack extension and speed increase but the failure mode is still crack propagation. However for small impact times the failure mode shifts from crack propagation to uniform debonding.

For cyclic loading computations revealed that the loading frequency affects crack growth. Resonating loading frequencies can dramatically accelerate crack growth while other frequencies have less pronounced influence. For very high frequencies results suggest that micro cracks may appear ahead of the crack tip sharply accelerating crack growth.

REFERENCES

- Freund, L. *Dynamic fracture mechanics*. Cambridge University Press, 1990.
- Needleman, A. Micromechanical modeling of interfacial decohesion. *Ultramicroscopy*, 40:203-214, 1992.
- Needleman, A. Numerical modeling of crack growth under dynamic loading conditions. *Computational mechanics*, 19:463-469, 1997.
- Roe, K. and Siegmund, T. An irreversible cohesive zone model for interface fatigue crack growth simulation. *Engineering Fracture Mechanics*, 70:2:209-232, 2003.
- Siegmund, T. and Needleman, A. A numerical study of dynamic crack growth in elastic-viscoplastic solids. *International Journal of Solids and Structures*, 34:7:769-787, 1997.
- Wang, B. and Siegmund, T. A computational analysis of size effects in fatigue failure. *Modelling and Simulation in Materials Science and Engineering*, 14:4:775-787, 2006.
- Xu, X. and Needleman, A. Numerical simulations of fast crack growth in brittle solids. *Journal of Mechanics and Physics of Solids*, 42:9:1397-1434, 1994.
- Zhou, F., Molinari, J. and Shioya, T. A rate-dependent cohesive model for simulating dynamic crack propagation in brittle materials. *Engineering Fracture Mechanics*, 72:1383-1410, 2005.